Journal of Materials Chemistry A

Accepted Manuscript

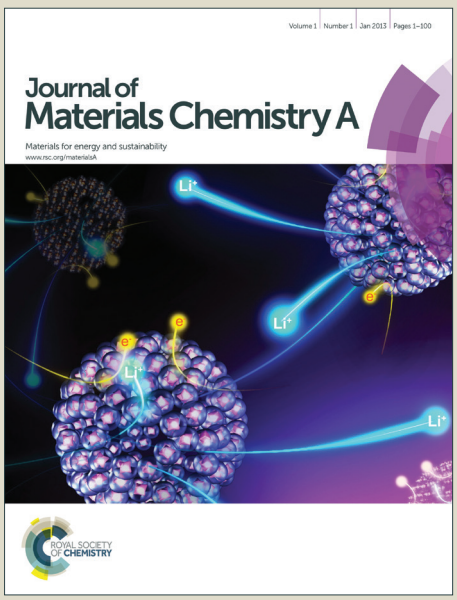

ROYAL SOCIETY OF CHEMISTRY

www.rsc.org/materialsA

Cite this: DOI: 10.1039/c0xx00000x

www.rsc.org/xxxxxx

ARTICLE TYPE

Highly dual-doped multilayer nanoporous graphene: efficient metal-free electrocatalysts for hydrogen evolution reaction†

Hongliang Jiang, Yihua Zhu,* Yunhe Su, Yifan Yao, Yanyan Liu, Xiaoling Yang and Chunzhong Li

Received (in XXX, XXX) Xth XXXXXXXXX 20XX, Accepted Xth XXXXXXXXX 20XX

DOI: 10.1039/b000000x

A bottom-up approach was introduced to prepare nitrogen and phosphorus dual-doped multilayer graphene with high dopant content and well-developed porosity, which leads to high catalytic activity in hydrogen evolution reaction with comparable onset overpotential (0.12 V) and Tafel slope (79 mV/dec) to some of traditional metallic catalysts.

Carbocatalysts (metal-free and heterogeneous carbon materials) has attracted tremendous attention due to their potential application in energy conversion and storage.[1] Among the carbon allotropes, graphene with its large surface area, high mechanical strength, and excellent electrical conductivity becomes an ideal candidate for electrochemical reactions.[2] However, the high chemical stability of pristine graphene implies low catalytic activity in electrochemical reactions, such as oxygen reduction reaction (ORR), oxygen evolution reaction (OER), and hydrogen evolution reaction (HER). To reduce the electrode overpotentials of these reactions, the further function of graphene becomes an efficient approach for tuning their catalytic activity.[3] Thereinto, the engineering of pristine graphene by chemical substitution of some carbon atoms with heteroatoms, such as N, B, P, and S, is a feasible way to tailor its electronic structure and (electro)chemical properties.[4] In these cases, it was found that the content and doped styles of the heteroatoms significantly impact their catalytic activity. On the other hand, the ineffective packing of 2D graphene sheets inevitably decreases the number of catalytically active sites. To address this issue, modifying the porosity of graphene catalysts is a promising way to enhance their electrocatalytic properties, which can maximize the electroactive surface area of catalysts and improve mass transfer during catalysis.[5] Although it has been demonstrated that heteroatom-doped graphene materials have shown excellent ORR and OER catalytic activity, most of their HER catalytic activity is not only much lower than that of Pt-based catalysts, but also inferior to that of the existing well-developed metallic catalysts (MoS_2, WS_2, $CoSe_2$, etc).[6] Therefore, the design and fabrication of metal-free graphene-based HER electrocatalysts with satisfactory activity and stability remain a big challenge.

Herein, a simple bottom-up approach was introduced to prepare highly dual-doped multilayer nanoporous graphene as efficient metal-free HER electrocatalysts via one-step solid-state reaction. In a typical synthesis of nitrogen and phosphorus dual-doped nanoporous graphene (NPG900), a mixture of urea, glucose and phosphoric acid with a mass ratio of 20:1:0.4 was annealed at 900 °C in argon flow at normal pressure (details available in Supporting Information). The formation of graphene nanosheets can be attributed to the sacrificial soft template of layered graphitic carbon nitride (g-C_3N_4) that is formed when urea is thermally treated at 350-600 °C.[7] At the temperature higher than 750 °C, the graphene nanosheets are liberated when the layered g-C_3N_4 template will be completely decomposed.[8] Urea was pyrolyzed and phosphoric acid was dehydrated to afford N and P source, respectively. Glucose was carbonized during the heating process to afford carbon source. The yield of the doped graphene is about 40% (calculated based on added carbon from glucose).

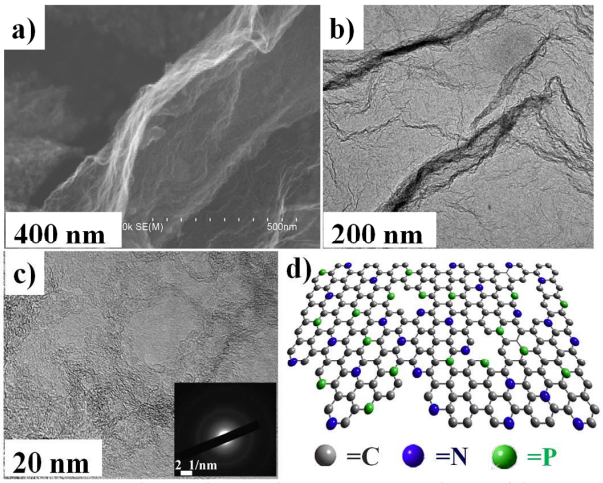

Figure 1. (a) SEM image, (b) TEM image, (c) HRTEM image of the NPG900 and the corresponding selected-area electron diffraction (SAED) pattern .(d) the structural model of highly dual-doped nanoporous graphene.

The structure and morphologies of the resulting samples were characterized by field-emission scanning electron microscopy (FE-SEM), transmission electron microscopy (TEM), and atomic force microscopy (AFM). Typical SEM images (Figure 1a and Figure S1a in the Supporting Information) confirm that the as-obtained NPG900 possesses two-dimensional (2D) nanosheets of carbon with entangled and crumpled morphology. The TEM image (Figure 1b) further reveals that the NPG900 is assemblies of crumpled, cross-linked but still transparent thin sheets. Along with different annealing temperature, the NPG800 and NPG1000 also present wrinkled graphene sheets similar to NG900, indicating that the annealing temperature (>800 °C) has little

effect on the morphology of NPG sheet (Figure S1b, c). The morphology observation shows that the as-prepared NG900 without phosphorus doping presents smoother sheets and fewer wrinkles compared with NPG. AFM measurement (Figure S2) demonstrates that the thickness of graphene nanosheets is about 2 nm, corresponding to 5~7 carbon atomic layers according to the theoretical thickness of a single-layer graphene (0.34 nm). The real structure of the NPG900 sample was revealed by high-resolution TEM (HRTEM). As shown in Figure 1c, the short-range contorted stripes are presented, which demonstrate the formation of very small and curved graphene sheets. Figure S3 demonstrates that these layers show a layer distance of about 0.34 nm but with poor crystallity. The SAED pattern of the same area (The inset of Figure 1c) also reveals that the typical hexagonal pattern for multicrystalline materials, which matches very broad XRD peaks (Figure S4). The pore characterization of the obtained samples was verified by measuring the nitrogen adsorption/desorption isotherms. Typical IV curves (Figure S5a) suggest micromesoporous structure, which is further demonstrated by the pore radius distributions of all samples (Figure S5b). The NPG900 shows highest BET surface area of 1102.1 m^2 g^{-1}, which is higher than those of highly reduced graphene oxides and solvothermally synthesized graphene assemblies.[9] The other samples have the BET surface area of 760.7 (NPG1000), 570.9 (NG900), and 391.2 m^2 g^{-1} (NPG800). The higher BET surface area of the NPG900 compared to that of NG900 indicates the dominating factor of phosphoric acid in increasing the porosity. To further demonstrate the role of phoshoric acid on increasing the porosity, the TEM images of NPG samples before or after ultrasonic exfoliation are shown in Figure S6. Some uniform phosphate nanoparticles were dispersed on the graphene sheets before ultrasonic exfoliation (Figure S6a). After ultrasonic exfoliation, some nanopores can be seen in the graphene sheets, which probably attributes to removal of phosphate nanoparticles (Figure S6b). Recently, Li et al. reported the preparation of boron- and nitrogen-codoped holey graphene monoliths.[8b] We believe that the formation of nanopores in the NPG is similar with the generation of nanoholes in the graphene sheets in the Li's work. The phosphate can enter into the interlayer space of layered C_3N_4 derived from the polymerization of urea due to the electrostatic interaction between phosphate groups and ammonia groups of carbon nitride. After further heat treatment at >800 ºC, the carbon nitride and phosphate in the interlayer space of layered C_3N_4 could completely decompose into nitrogen-and phosphorus-containing species for doping reactions. Meanwhile, a large amount of gas from the decomposition of the carbon nitride and phosphate prompts the formation of crumpled structure and high specific surface area. From the above-mentioned results, the structural model of highly dual-doped nanoporous graphene is shown in Figure 1d.

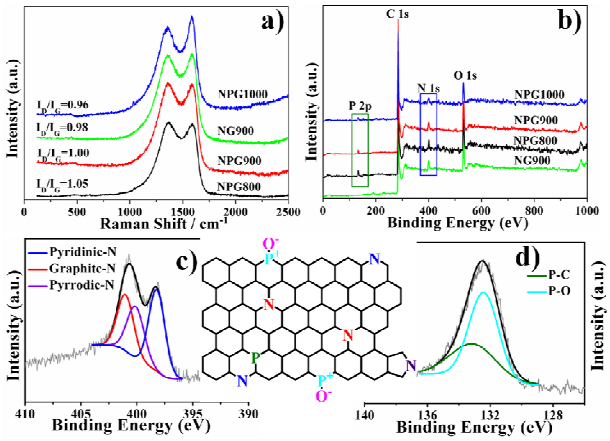

Figure 2. (a) The Raman spectra and (b) wide XPS survey of all samples. The high resolution (c) N 1s XPS and (d) P 2p spectra of the NPG900. The inset between Figure 2c and 2d is schematic representation of nitrogen and phosphorus doping in NPG.

To further demonstrate structural defects of as-prepared samples, Raman spectroscopy and X-ray photoelectron spectroscopy (XPS) measurements were conducted. A G-band at 1578 cm^{-1} in the 532 nm Raman spectrum (Figure 2a) of the samples supports the formation of graphitic carbon. Similar to nanometer-sized graphite particles and chemically modified graphene flakes, the sample has also a broad D-band centered at 1356 cm^{-1}, underlining the presence of disorder and a certain amount of heteroatoms. The intensity ratio of the D to the G band (I_D/I_G) decreases from 1.05 (NPG800) to 0.96 (NPG1000), indicating enhanced graphitization at higher temperature. The XPS survey spectrum of all samples given in Fig. 2b directly reveals the presence of C 1s, N 1s, P 2p, and O 1s without any other element. The C 1s peaks for the samples (Figure S7) center at approximately 284.6 eV, with a tail at higher binding energies, which is a common effect for doped carbon materials.[8a] The total heteroatom content of NPG900 is 3 atom% and 11 atom% for P and N, respectively (Table S1), which is higher than that of most doped carbon materials. Both the contents of N and P decrease with increasing the annealing temperature, indicating that N and P dopants may become unstable and are removed from the NPG carbon framework at elevated temperature. High resolution XPS spectra were conducted to reveal the bonding configurations of N and P in the NPG900 (Figure 2c and 2d). The N 1s band can be deconvoluted into three bands, which are pyridinic-N (398.3 eV), pyrrolic-N (400.1 eV), and graphitic-N (401.2 eV), respectively. The P 2p band can be deconvoluted into two bands, which are P-O bonding (133.8 eV) and P-C bonding (132.7 eV). The schematic representation of three types of nitrogen and two types of phosphorus doping in NPG is shown in the inset between Figure 2c and 2d. These results further demonstrate that N and P heteroatoms have been doped into the carbon network.

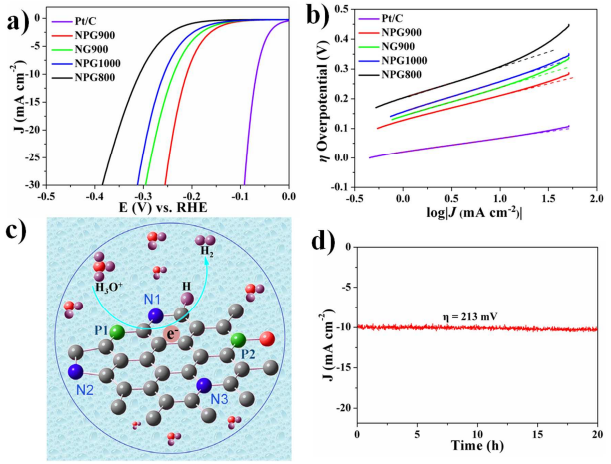

Figure 3. (a) Polarization curves of various samples and (b) the corresponding Tafel plots. (c) A schematic representation of the HER process on the surface of NPG. The gray balls represent C atoms, green for P, blue for N, red for O and purple for H. (d) Time dependence of cathodic current density for NPG900 over 20 h at fixed overpotentials of 213 mV.

The HER catalytic activity of all samples is evaluated in a typical three electrode cell setup with 0.5 M H_2SO_4 solution (see the Supporting Information for experimental details). Figure 3a shows typical polarization curve (J-V plot) with a sweep rate of 2 mV s^{-1}. Commercial Pt/C catalyst exhibits expected HER activity with negligible overpotential. The N and P dual-doped NPG900 sample presents a low onset overpotential (η) of *ca.* 120 mV and achieves current densities of 10 mA cm^{-2} at overpotentials of *ca.* 213 mV, which surpass the summed value of single doped NG900 and other dual-doped samples (NPG800 and NPG1000) prepared in different temperature (Figure 3a, Figure S8, and Table S2). To further understand the reaction mechanism of HER activity, Tafel slopes, determined for the rate-limiting step of HER, are used to interpret possible elementary steps involved. As show in Figure 3b and Table S2, the Tafel slopes for as-prepared catalysts are *ca.* 80-100 mV/dec (NPG900 shows the lowest value of 79 mV/decade), indicating that the HER mechanism of our catalyst follows Volmer-Heyrovsky reaction where an initial proton adsorption is the rate-determining step (Figure 3c).[10] In addition, exchange current densities of various samples were also obtained by the extrapolation of Tafel plots. As listed in Table S2, NPG900 displays the largest exchange current density of 0.0243 mA cm^{-2}. The high electrode kinetic metrics of NPG900 (including onset overpotential of 120 mV, the tafel slope of 79 mV/dec, and exchange current density of 0.0243 mA cm^{-2}) is comparable to that of traditional metallic catalysts (Table S3).

Generally, the overall HER pathway, $2H^+ + 2e^- \rightarrow H_2$, can be described by a three-state diagram comprising of an initial state $H^+ + e^-$, an intermediate adsorbed H*, and the final product H_2. Previous work have demonstrated that a good catalyst of the HER should have a moderate free energy for H* adsorption (ΔG(H*)) to compromise the reaction barriers of the adsorption and desorption steps.[4d, 11] As reported by Qiao and co-workers,[11] Both N and/or P incorporation could reduce the ΔG(H*) values to enhance the initial H* adsorption, in which pyridinic N and P dual-doped model demonstrates the lowest $|\Delta G(H^*)|$ value, indicating its highest HER activity. Bao and co-workers reported that activated carbon nanotube with FeCo encapsulated and N doping showed high activity and long-term durability towards HER. Density function theory (DFT) calculations indicated that the introduction of metal and nitrogen dopants can synergistically optimize the electronic structure of the CNTs and the adsorption free energy of H atom on CNTs, and therefore promote the HER.[12] It is believed that our work also follows the principle of the above. The coupling of these N dopants with the P dopants has themost favorable H* adsorption desorption property, leading to enhanced electrocatalytic activity compared with single doped samples. On the other hand, the concentration of these dopants linked to preparation temperature notably influences the catalytic activity. The NPG800 sample prepared at lower temperature has lower electrical conductivity which blocks the charge transfer. The NPG1000 sample prepared at high temperature is lack of catalytically active sites. Accordingly, the NPG900 sample shows optimized HER activity. Stability is a critical aspect in the development of electrocatalysts. For this reason, we further probed the durability of the NPG900 catalyst by long-term tests. Figure 3d suggests that the catalyst maintains its catalytic activity for at least 20 hours by the time dependence of the current density at fixed overpotentials of 213 mV, which is further verified by the negligible loss of current density after 1000 cycles compared to the initial polarization curve (Figure S9). Such robust stability may attribute to strong covalent C-N (or C-P) bonds and well-developed porosity.

Conclusions

In summary, nitrogen and phosphorus dual-doped multilayer graphene was successfully prepared via one-step solid-state reaction of urea, glucose and phosphoric acid. This strategy leads to crumpled and cross-linked graphene sheets with high dopant content and well-developed porosity. We further demonstrate the use of as-prepared materials as novel HER electrocatalysts. The optimized NPG900 shows comparable onset overpotential (0.12 V), Tafel slope (79 mV/dec) and exchange current density (0.0243 mA cm^{-2}) to some of traditional metallic catalysts. Stability tests though long-term potential cycles and extended electrolysis confirm the exceptional durability of the catalyst. More importantly, further functionalization can be realized by the introduction of transition metals (Fe, Co, Ni, etc) and then the application can extend to the other electrochemical reactions, such as oxygen reduction reaction (ORR), oxygen evolution reaction (OER), etc.

Acknowledgements

This work was supported by the National Natural Science Foundation of China (21471056, 21236003, 21206042, and 21176083), the Basic Research Program of Shanghai (13NM1400700, 13NM1400701), and the Fundamental Research Funds for the Central Universities.

Notes and references

Key Laboratory for Ultrafine Materials of Ministry of Education, School of Materials Science and Engineering, East China University of Science and Technology, Shanghai 200237, China. Fax: +86 21 6425 0624; Tel: +86 21 6425 2022; E-mail: yhzhu@ecust.edu.cn (Y. Zhu).

† Electronic Supplementary Information (ESI) available: experimental details and other supporting results including SEM images, TEM images, XRD, the nitrogen adsorption/desorption isotherms, etc. See DOI: 10.1039/b000000x/

1 a) X.-K. Kong, C.-L. Chen and Q.-W. Chen, *Chem. Soc. Rev.*, 2014, **43**, 2841. b) Y. Li, W. Zhou, H. Wang, L. Xie, Y. Liang, F. Wei, J.-C. Idrobo, S. J. Pennycook and H. Dai, *Nat. Nanotechnol.*, 2012, **7**, 394. c) S. Chen, J. Duan, M. Jaroniec and S. Qiao, *Adv. Mater.*, 2014, **26**, 2925. d) H. Jiang, Y. Zhu, Q. Feng, Y. Su, X. Yang and C. Li, *Chem. Eur. J.*, 2014, **20**, 3106.

2 a) A. Ambrosi, C. K. Chua, A. Bonanni and M. Pumera, *Chem. Rev.*, 2014, **114**, 7150. b) J. Jin, F. Pan, L. Jiang, X. Fu, A. Liang, Z. Wei, J. Zhang and G. Sun, *ACS Nano*, 2014, **8**, 3313. c) Z. Lin, G. Waller, Y. Liu, M. Liu and C. Wong, *Adv. Energy Mater.*, 2012, **2**, 884.

3 a) J. Liang, X. Du, C. Gibson, X. Du and S. Qiao, *Adv. Mater.*, 2013, **25**, 6226. b) X. Wang, J. Wang, D. Wang, S. Dou, Z. Ma, J. Wu, L. Tao, A. Shen, C. Ouyang, Q. Liua and S. Wang, *Chem. Commun.*, 2014, **50**, 4839. c) J. Tian, Q. Liu, A. M. Asiri, K. A. Alamry and X. Sun, *ChemSusChem*, 2014, **7**, 2125. d) W. Cui, Q. Liu, N. Cheng, A. M. Asiricd and X. Sun, *Chem. Commun.*, 2014, **50**, 9340.

4 a) Y. Gong, H. Fei, X. Zou, W. Zhou, S. Yang, G. Ye, Z. Liu, Z. Peng, J. Lou, R. Vajtai, B. Yakobson, J. Tour and P. Ajayan, *Chem. Mater.*, 2015, **27**, 1181. b) J. Duan, S. Chen, M. Jaroniec and S. Qiao, *ACS Nano*, 2015, **9**, 931. c) Y. Zheng, Y. Jiao, Y. Zhu, L. Li, Y. Han, Y. Chen, A. Du, M. Jaroniec and S. Qiao, *Nat. Commun.*, 2014, **5**, 3783. d) Y. Ito, W. Cong, T. Fujita, Z. Tang and M. Chen, *Angew. Chem. Int. Ed.*, 2015, **54**, 2131. e) X. Wang, J. Wang, D. Wang, S. Dou, Z. Ma, J. Wu, L. Tao, A. Shen, C. Ouyang, Q. Liua and S. Wang, *Chem. Commun.*, 2014, **50**, 4839.

5 a) Z. Wu, S. Yang, Y. Sun, K. Parvez, X. Feng and K. Müllen, *J. Am. Chem. Soc.*, 2012, **134**, 9082. b) Z. Chen, W. Ren, L. Gao, B. Liu, S. Pei and H. Cheng, *Nat. Mater.*, 2011, **10**, 424. c) Y. Zhu, S. Murali, M. Stoller, K. Ganesh, W. Cai, P. Ferreira, A. Pirkle, R. Wallace, K. Cychosz, M. Thommes, D. Su, E. Stach and R. Ruoff, *Science*, 2011, **332**, 1537.

6 a) P. Du and R. Eisenberg, *Energy Environ. Sci.*, 2012, **5**, 6012. b) M. Lukowski, A. Daniel, F. Meng, A. Forticaux, L. Li and S. Jin, *J. Am. Chem. Soc.*, 2013, **135**, 10274. c) Y. Yu, S. Huang, Y. Li, S. Steinmann and W. Yang and L. Cao, *Nano Lett.*, 2014, **14**, 553. d) L. Cheng, W. Huang, Q. Gong, C. Liu, Z. Liu, Y. Li and H. Dai, *Angew. Chem. Int. Ed.*, 2015, **53**, 7860. e) M. Gao, J. Liang, Y. Zheng, Y. Xu, J. Jiang, Q. Gao, J. Li and S. Yu, *Nat. Commun.*, 2015, **6**, 5982.

7 a) F. Pan, J. Jin, X. Fu, Q. Liu and J. Zhang, *ACS Appl. Mater. Interfaces*, 2013, **5**, 11108. b) J. Liu, T. Zhang, Z. Wang, G. Dawson, W. Chen, *J. Mater. Chem.*, 2011, **21**, 14398.

8 a) X. Li, S. Kurasch, U. Kaiser and M. Antonietti, *Angew. Chem. Int. Ed.*, 2012, **51**, 9689. b) X. Li and M. Antonietti, *Angew. Chem. Int. Ed.*, 2013, **52**, 4572. c) J. Jin, F. Pan, L. Jiang, X. Fu, A. Liang, Z. Wei, J. Zhang and G. Sun, *ACS Nano*, 2014, **8**, 3313.

9 a) S. Park and S. Ruoff, *Nat. Nanotechnol.*, 2009, **4**, 217. b) M. Choucair, P. Thordarson and J. Stride, *Nat. Nanotechnol.*, 2009, **4**, 30.

10 a) Y. Li, H. Wang, L. Xie, Y. Liang, G. Hong and H. Dai, *J. Am. Chem. Soc.*, 2011, **133**, 7296. b) L. Liao, S. Wang, J. Xiao, X. Bian, Y. Zhang, M. Scanlon, X. Hu, Y. Tang, B. Liu and H. Girault, *Energy Environ. Sci.*, 2014, **7**, 387.

11 Y. Zheng, Y. Jiao, L. Li, X. Tan, Y. Chen, M. Jaroniec and S. Qiao, *ACS Nano*, 2014, **8**, 5290.

12 J. Deng, P. Ren, D. Deng, L. Yu, F. Yang and X. Bao, *Energy Environ. Sci.*, 2014, **7**, 1919.

Graphical Abstract

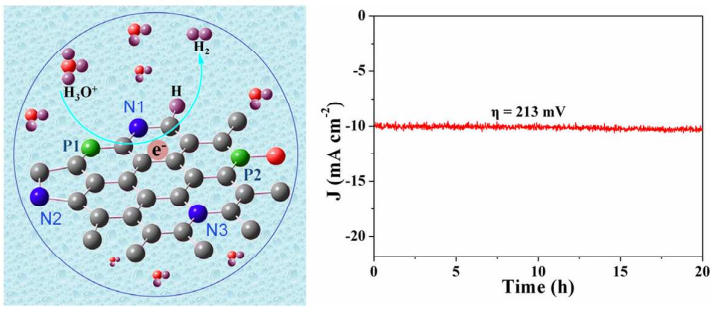

Nitrogen and phosphorus dual-doped multilayer graphene exhibits an excellent and robust hydrogen evolution reaction (HER) electrocatalytic performance.